Structure *19*

Supplemental Information

Interferon-Inducible Protein 16: Insight into the Interaction with Tumor Suppressor p53

Jack C.C. Liao, Robert Lam, Vaclav Brazda, Shili Duan, Mani Ravichandran, Justin Ma, Ting Xiao, Wolfram Tempel, Xiaobing Zuo, Yun-Xing Wang, Nickolay Y. Chirgadze, and Cheryl H. Arrowsmith

Figure S1

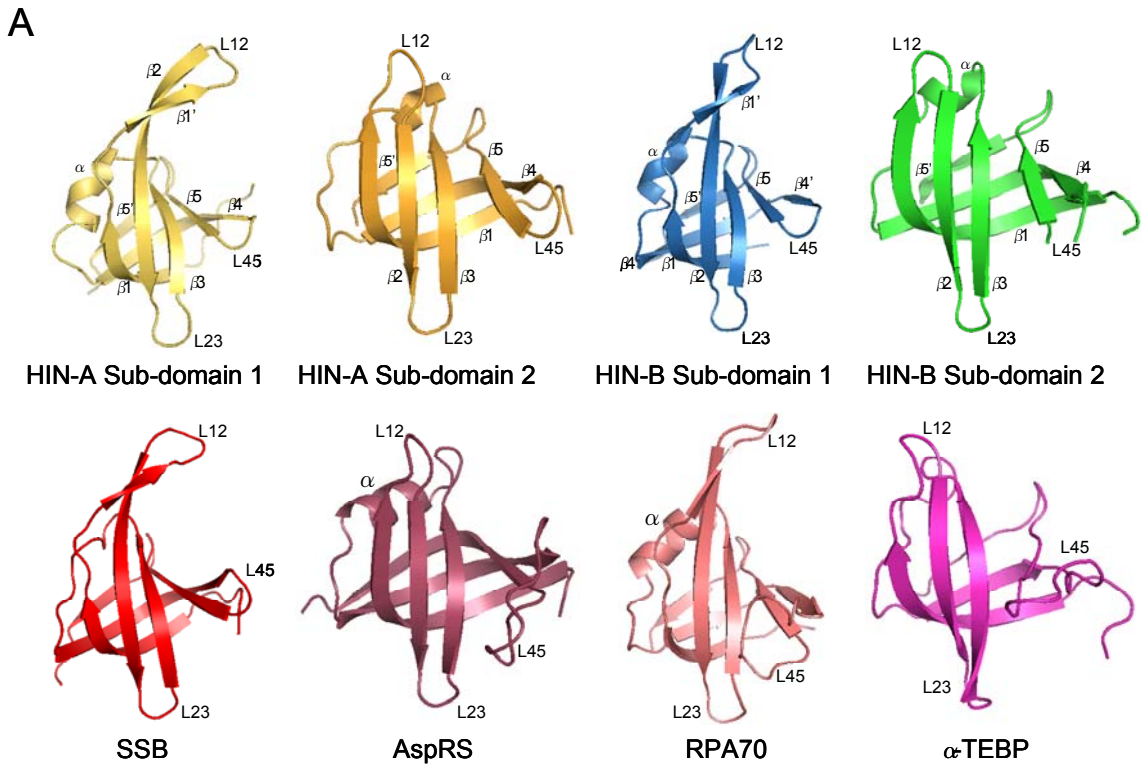

Figure S1 (related to Figure 1B). IFI16 HIN sub-domains are OB folds
(A) Structural comparison of IFI16 HIN sub-domains to OB fold-containing proteins. SSB: single-stranded DNA-binding protein from *Sulfolobus solfataricus*, PDB: 1O7I. AspRS: Aspartyl-tRNA synthetase from *E. coli*, PDB: 1L0W. RPA70: DNA Binding Domain (DBD)-A of the 70 kDa subunit of the human Replication Protein A, PDB: 1FGU. α-TEBP: first OB fold domain of the telomere end-binding protein α-subunit, PDB: 2I0Q. (B) Superimposition of the IFI16 HIN-A (Left) or HIN-B (Right) domain with two tandem DBDs of DNA complexed form of RPA70, PDB: 1JMC. *Yellow*: HIN-A; *Blue*: HIN-B; *Pink*: RPA70. (C) Overlay of IFI16 HIN-A and HIN-B structures. *Yellow*: HIN-A; *Blue*: HIN-B.

Figure S2

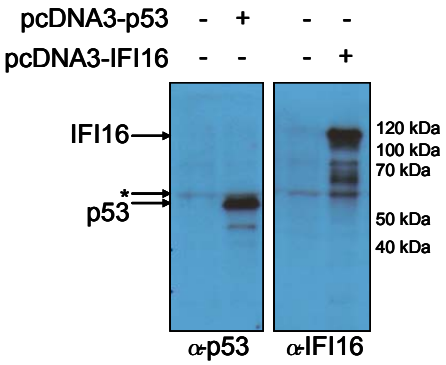

Figure S3

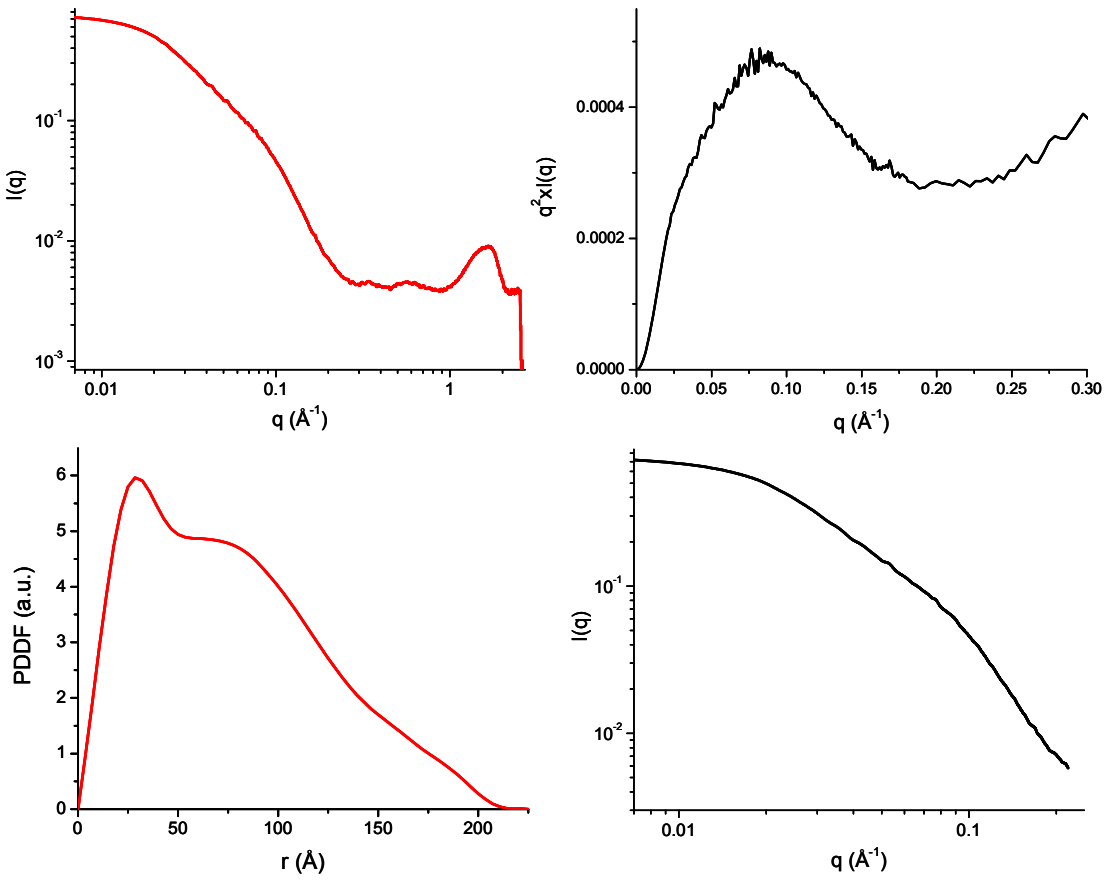

Figure S2 (related to Figure 7). **H1299 cells did not express endogenous p53 or IFI116**
H1299 cells were transfected with empty vector or vector containing p53 or IFI16. Lysates were detected for p53 or IFI16 protein by α-p53 (1801) or α-IFI16 (Abcam). Asterisk indicates background/contaminant.

Figure S3 (related to Figure 8). **SAXS analysis of IFI16**
(A) The total scattering profile of full-length IFI16. (B) Kratky plot. (C) Pair distance distribution function. (D) The portion of scattering profile used in molecular envelope calculation of full-length IFI16.

SUPPLEMENTAL EXPERIMENTAL PROCEDURES

Data Collection and Structure Determination of IFI16 HIN-A

Diffraction datasets from crystals cryo-protected using a mixture containing mother liquor with 17% glycerol (v:v) and flash-frozen in liquid nitrogen were collected using the ADSC QUANTUM 210 CCD detector at IMCA-CAT beam line 17-ID at the Advanced Photon Source. The data were integrated and scaled using HKL2000 suite (Otwinowski and Minor, 1997). The structure was determined using the single-wavelength anomalous dispersion (SAD) method utilizing the anomalous signal from selenium atoms. Using diffraction data between 47 Å and 2.6 Å resolution, the positions of 24 selenium atoms were found by heavy-atom refinement and phasing using maximum-likelihood-based algorithm as implemented in the autoSHARP program suite (Vonrhein *et al*. 2006). Phase improvement by density modification generated an interpretable experimental SAD map at 2.0 Å, allowing an initial model to be built using ARP/wARP (Langer *et al*., 2008). The model was subsequently improved through iterative cycles of manual building using COOT (Emsley and Cowtan, 2004) and restrained refinement against a maximum-likelihood target with 5% of the reflections randomly excluded as an R_{free} test set. All refinement steps were performed using REFMAC as implemented in the CCP4 program suite (The CCP4 Suite, 1994). The final model, containing four monomers of IFI16 in the asymmetric unit, was refined to an R_{work} of 21.1% and R_{free} of 26.0% at 2.0 Å resolution including 159 water molecules. All residues are in the most favored and additionally allowed regions of the Ramachandran plot. Data collection, phasing and structure refinement statistics are summarized in **Table 1**.

Data Collection and Structure Determination of IFI16 HIN-B

Native datasets from crystals cryo-protected in 40% PEG 4000 were collected using the ADSC QUANTUM 210 CCD detector at beam line 1A at the Cornell High Energy Synchrotron Source. The structure was determined by molecular replacement using the program Molrep as implemented in the CCP4 program suite (The CCP4 Suite, 1994) and an initial search model consisting of IFI16 HIN-A with all solvent molecules removed. Both molecules of HIN-B in the asymmetric unit were successfully located and subsequently refined and rebuilt using the REFMAC (The CCP4 Suite, 1994) and COOT (Emsley and Cowtan, 2004) software programs, respectively. The final model including 17 water molecules was refined to an R_{work} of 22.9% and R_{free} of 29.2% at 2.35 Å resolution. All residues are in the most favored and additionally allowed regions of the Ramachandran plot. Data collection and structure refinement statistics are summarized in **Table 1**.

SAXS Experiments, Data Analysis, and Bead Model Reconstruction

The wavelength of X-ray radiation was set as 0.689 Å and the scattered X-ray photons were recorded with a charge-coupled device X-ray detector (Mar Research). An X-ray flow cell

made of a cylindrical quartz capillary with a diameter of 1.5 mm and a wall of 10 μm was used. The X-ray beam with size of 0.1 × 0.2 mm^2 was adjusted to pass through the center of the cell. The exposure time was set to 0.4 – 0.6 seconds to avoid detector saturation and radiation damage. Potential radiation damage was further reduced by flowing the samples. The range of momentum transfers $q = 4\pi \sin\theta/\lambda$, where 2θ is the scattering angle, were set between 0.006 – 0.250 $Å^{-1}$ and 0.1 – 2.6 $Å^{-1}$ for SAXS and WAXS, respectively.

Twenty images were taken for each sample or buffer solution to get good statistics. The 2-D scattering images of buffers and samples were azimuthally averaged after solid angle correction and then normalized with the intensity of the incident X-ray beam. The resulting 1-D scattering data sets were averaged before buffer background subtraction. The background subtractions were performed using a procedure describe previously (Zuo *et al*., 2010).

The radius of gyration (R_g) was calculated from data at low q values in the range of $qR_g < 1.2$, using the Guinier approximation (Eq. 1):

$$\ln I(q) = \ln(I(0)) - R_g^2 q^2 / 3 \qquad \text{(Eq. 1)}$$

The R_g values using this reciprocal space method were 56 ± 2 Å for the IFI16 protein. The scattering intensities at and near $q = 0$ were extrapolated with the Guinier equation. The final scattering data of IFI16 with a Guinier extrapolation was displayed in **Figure S2A**. The partial bell-shaped Kratky plot (**Figure S2B**), q^2xI(q) vs q, and the relatively large Rg value indicate that IFI16 is elongated.

The PDDF, *p(r)*, in the real space, was calculated using the GNOM program (Svergun, 1992), which uses an indirect Fourier transform and a real space perceptual criteria based on a solid sphere. To avoid under-estimation of the molecular dimension and consequent distortion in low resolution structural reconstruction, the parameter R_{max}, the upper end of distance r, was manually scanned in the range of 180 – 240 Å with a 5 Å interval, and chosen such that the resulting PDDF has a short, near zero-values tail at large r. The maximum distances (D_{max}) were estimated as 210 ± 10 Å from the PDDF for the full-length IFI16 molecule (**Figure S2C**).

We used the program DAMMIF (Franke and Svergun, 2009), a fast version of the DAMMIN program (Svergun, 1999), to obtain an approximate molecular envelope. In DAMMIF, a spherical space with a radius of R_{max}, read from the PDDF result, was initially built and filled with multiple-phase small beads or dummy atoms. To avoid distortion caused by possible under-estimation of D_{max}, DAMMIF can automatically adjust the value of R_{max} during the calculation. At each step, the envelope evolved by randomly phasing a dummy-atom in (as a part of the molecule) or out (as a part of the solvent). A simulated annealing algorithm is employed in DAMMIF/DAMMIN for driving the envelope evolution, by reducing the discrepancy between the experimental and calculated scattering curves during the annealing process. All reconstructions for IFI16 were run in the "slow" mode, with a default setting of DAMMIF. The resulting structural models were subjected to averaging using the program package DAMAVER (Petoukhov *et al*., 2007). In this program, the normalized spatial discrepancy (NSD) values between each pair of models were computed. The model with the lowest average NSD with respect to the rest of models was chosen as the reference model. The remaining models were superimposed onto the reference model using SUPCOMB (Kozin and Svergun, 2001) except that possible outliers identified by NSD criteria were discarded. The dummy atoms of these superimposed models were remapped onto a densely packed grid of atoms with each grid point marked with its occupancy factor. The grids with non-zero occupancies were chosen to generate a final consensus model with the volume equal to the average excluded volume of all the models. Scattering data in a q range of 0 – 0.22 $Å^{-1}$ (**Figure S2D**), which reflect the global shape without significant undesired influence from the internal structure, were used in DAMMIF calculations. Thirty-two independent DAMMIF runs were

performed and the resulting bead models were subjected to averaging by DAMAVER. The R_f values, as defined in the following:

$$R_f^2 = \sum_q [(sc * I_{\mathrm{mod}}(q) - I_{\mathrm{exp}}(q)) * q^2]^2 \Big/ \sum_q [I_{\mathrm{exp}}(q) * q^2]^2 \qquad \text{(Eq. 2)}$$

were in the range of 0.004 – 0.006, indicating good match between the experimental scattering data and the calculated ones for individual models, and the average NSD for those bead models was 0.82 ± 0.03, which indicate the excellent convergences in both individual DAMMIN fits and overall bead model ensembles for each sample.

SUPPLEMENTAL REFERENCES

Emsley P, Cowtan K. (2004). Coot: model-building tools for molecular graphics. Acta Crystallogr D 60, 2126-2132.

Franke, D., and Svergun, D. I. (2009). DAMMIF, a program for rapid ab-initio shape determination in small-angle scattering, J Appl Cryst *42*, 342–346.

Kozin, M. B., and Svergun, D. I. (2001). Automatedmatching of high- and low-resolution structural models, J Appl Cryst *34*, 33–41.

Langer, G., Cohen, S.X., Lamzin, V.S. & Perrakis, A. (2008). Automated macromolecular model building for X-ray crystallography using ARP/wARP version 7. Nature Protocols *3*, 1171-1179.

Otwinowski Z, Minor W. Processing of X-ray Diffraction Data Collected in Oscillation Mode (1997). Methods Enzymol *276*, 307-326.

Petoukhov, M. V., Konarev, P. V., Kikhney, A. G., and I.Svergun, D. (2007). ATSAS 2.1 – towards automated and websupported small-angle scattering data analysis, J Appl Cryst *40*, s223–s228.

Svergun, D. I. (1992). Determination of the regularization parameter in indirect-transform methods using perceptual criteria, J Appl Cryst *25*, 495-503.

Svergun, D. I. (1999). Restoring low resolution structure of biological macromolecules from solution scattering using simulated annealing. Biophys J *76*, 2879-2886.

The CCP4 Suite: Programs for Protein Crystallography. (1994). Acta Crystallogr D 50, 760-763.

Vonrhein C, Blanc E, Roversi P, Bricogne G. (2006). Automated Structure Solution With autoSHARP. Methods Mol Biol *364*, 215-230.

Zuo, X., Wang, J., Yu, P., Eyler, D., Xu, H., Starich, M. R., Tiede, D. M., Simon, A. E., Kasprzak, W., Schwieters, C. D., Shapiro, B. A., and Wang, Y. X. (2010). Solution structure of the cap-independent translational enhancer and ribosome-binding element in the 3’ UTR of turnip crinkle virus. Proc Natl Acad Sci U S A *107*, 1385-1390.